UDK 544.3.032.2:669.018
Original scientific article/Izvirni znanstveni članek

ISSN 1580-2949
MTAEC9, 55(2)269(2021)

EFFECT OF C-Mn PARTITIONING ON THE MICROSTRUCTURE AND MECHANICAL PROPERTIES OF TRIP STEEL

VPLIV PRERAZPOREDITVE C IN Mn NA MIKROSTRUKTURO IN MEHANSKE LASTNOSTI TRIP JEKLA

Cainian Jing*, Qiteng Lei, Tao Lin, Daomin Ye, Cong Wu, Jingrui Zhao, Shubo Xu

School of Materials Science and Engineering, Shandong Jianzhu University, Jinan, Shandong, China

Prejem rokopisa – received: 2020-09-15; sprejem za objavo – accepted for publication: 2021-01-08

doi:10.17222/mit.2020.181

In this paper, the TRIP590 steel was used for C-Mn partitioning. The influence of C-Mn partitioning on the microstructure and mechanical properties of the steel was studied. SEM, EPMA, XRD and tensile tests were used to characterize the microstructure of the tested steel, calculate the content of retained austenite, and analyze the enrichment of C atoms and Mn atoms and mechanical properties. The results show that there was a lot of lath martensite and scattered ferrite in the microstructures of the Q&P steel and C-Mn partitioning steel. After C-Mn partitioning, the content of ferrite was increased. The enrichment of C and Mn in the C-Mn partitioning steel was relatively apparent, and the concentration of the atoms in the center of martensite was significantly higher than at the boundary between martensite and ferrite. Mn-rich areas were also C-rich areas. Compared with the Q&P steel, the C-Mn partitioning steel had a larger amount of retained austenite, higher elongation and PSE.

Keywords: product of strength and elongation, element enrichment, Q&P process, C-Mn partitioning, retained austenite

V članku avtorji opisujejo proces prerazporeditve C in Mn v TRIP590 jeklu. Avtorji so študirali vpliv prerazporeditve na mikrostrukturo in mehanske lastnosti izbranega jekla. Za karakterizacijo njegove mikrostrukture, izračun vsebnosti zaostalega austenita, analize obogatitve z C in Mn atomi so uporabili SEM, EPMA, XRD in natezne preizkuse. Rezultati analiz so pokazali, da je v mikrostrukturi Q&P jekla precej letvastega martenzita in razpršenega ferita. Po prerazporeditvi Mn in C pa je narasla vsebnost ferita. Obogatitev s C in Mn je relativno navidezna v C-Mn jeklu s prerazporeditvijo obeh in koncentracija atomov v središču martenzita je bistveno višja kot na mejah med martenzitom in feritom. Z Mn bogata območja so bogata tudi s C. Primerjava z Q&P jeklom ima jeklo s C-Mn preporazdelitvijo večjo vsebnost zaostalega austenita, večji raztezek in PSE.

Ključne besede: produkt trdnosti in raztezka, obogatitev elementa, Q&P proces, C-Mn proces prerazporeditve, zaostali austenit

1 INTRODUCTION

The World Steel Association divides high-strength steels for automobiles into two major categories, based on differences in strengthening mechanisms, namely traditional high-strength steels and advanced high-strength steels (AHSSs).[1] At present, AHSSs include three generations: transformation-induced plasticity steel (TRIP steel),[2] twinning-induced plasticity steel (TWIP steel),[3] and quenching and partitioning steel (Q&P steel).[4] In 2003, J. Speer et al.[5] proposed the Q&P process and established a constrained para-equilibrium model to study the problem of the C-element partitioning of the test steel between the temperature of the martensite starting point (M_s) and the martensite ending point (M_f). In recent years, the third-generation AHSS, represented by medium-manganese steel and Q&P steel has developed rapidly.[6] The typical production of the Q&P steel can be a "one-step" Q&P process and a "two-step" Q&P process.[7] The "one-step" Q&P process includes quick heating of the steel to the austenite zone, its transition to the temperature between M_s and M_f for C partitioning and finally its quenching to room temperature. The "two-step" Q&P process also includes its transition to the fully austenitized steel, to the temperature between M_s and M_f, and then the performance of C-partitioning treatment at a temperature higher than this temperature and finally its quenching to room temperature. The microstructure of the material is composed of a martensitic matrix and carbon-enriched austenite retained after the Q&P process.[8]

The PSE is the product of tensile strength and elongation.[9] In addition to excellent tensile-stress resistance, high-strength steel must also exhibit a good plasticity. So the PSE is usually used to evaluate the performance of high-strength steel. TRIP steel is designed based on the traditional high-strength steels by introducing retained austenite, which greatly improves the workability and cold-forming performance.[10] TRIP steel is often used for automobile safety and structural parts due to its high PSE and good fatigue resistance. When a car is crashing, the high-strength martensite in the steel can resist its deformation,[11] undergoing a TRIP effect.[12] The retained austenite is transformed into harder martensite, significantly improving the safety performance of cars. Most researches on the TRIP steel have been focused on hot-rolling and cold-rolling properties[13] and isothermal

*Corresponding author's e-mail:
jcn@sdjzu.edu.cn (Cainian Jing)

transformation rules.[14] The influence of the diffusion of C-atoms and Mn-atoms on the TRIP steel structure and mechanical properties is also important. As the main strengthening element of martensite, carbon can reduce the M_s and stabilize the retained austenite. As the vital element for stabilizing austenite, manganese can expand the austenite zone.[15] C. H. Song et al.[16] proposed that carbon atoms at the austenite interface can attract manganese atoms. Y. Q. Tian et al.[17] studied the effects of C and Mn on the stability of the retained austenite in bainitic steel. It was confirmed that the diffusion of C and Mn atoms could increase the retained-austenite stability, thereby improving the performance of steel.[18] To further study the atom-diffusion behavior in TRIP steel, in the two-phase region, and the interaction between C-atoms and Mn-atoms, in this work, the optimized Q&P process was used to heat treat TRIP590 steel. This process combines the C-Mn partitioning process with the traditional Q&P process, making the C partitioning and Mn partitioning have a far-reaching effect. Moreover, the theoretical basis was provided for the development of AHSS by analyzing the influence of the C-Mn partitioning process on the atom-partitioning behavior, microstructure and mechanical properties.

2 EXPERIMENTAL PART

The TRIP590 steel with a thickness of 1.5 mm was used in this work. **Table 1** shows the main composition of the tested steel.

Table 1: Main chemical composition of the tested steel (w/%)

Component	C	Mn	Si	Al	Cr	Ti	S	P	B
Content	0.11	1.50	1.16	0.043	0.024	0.01	0.001	0.008	0.003

The M_s of the tested steel is 390 °C. The austenite start point (A_{c1}) is at 720 °C and the austenite end point (A_{c3}) is at 880 °C.[19]

Figure 1 shows the heat-treatment process. **Figure 1a** shows the Q&P process: the tested steel was heated and austenitized in a resistance furnace at a temperature of 940 °C and held for 5 min, then quickly transferred to a salt bath with a temperature of 240 °C, held there for 10–50 s for C partitioning and finally quenched to room temperature. **Figure 1b** shows the C-Mn partitioning process: during the first step, the tested steel was quickly heated in the resistance furnace to a two-phase (austenite + ferrite) zone temperature of 820 °C and held for 20 min. In the second step, the tested steel was heated in the resistance furnace at a temperature of 940 °C and held for 5 min, then quickly transferred to a salt bath with a temperature of 240 °C, held there for 10–50 s for C partitioning and finally quenched to room temperature. The cooling medium for both processes was water.

In this experiment, an MXQ1700-30 type high-temperature box-type atmosphere furnace and an SG2-5-10 type salt-bath furnace were used to process the test steel in different ways. The tested steel was cut, mosaiced, coarsely ground, finely ground and polished.

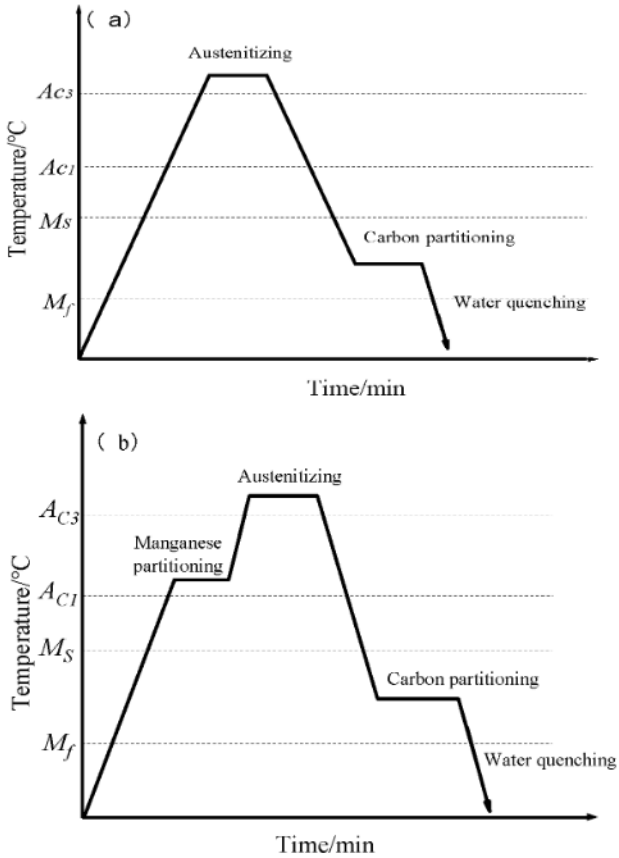

Figure 1: Heat-treatment curves for the experiment: a) Q&P process, b) C-Mn partitioning process

A scanning observation of the microstructure and tensile-fracture morphology of the tested steel was carried out on a Japanese JSM-7610F high-resolution scanning electron microscope (SEM). The SEM scanning-test object was the cross-section of the tested steel. SEM specimens were etched with 4-pct Nital solution. This experiment used a Japanese EPMA-1600 electron-probe X-ray micro-analyzer (EPMA) to characterize the C-Mn partitioning effect. The working voltage used in the test was 15 kV, the scanning area was (20×15) μm and the scanning-area magnification was 4000×.

In this experiment, the German Bruker D8 Advance CuK_α target X-ray diffraction analyzer (XRD) was used to identify the phase of the tested steel; combined with Equation (1),[20] X-ray diffraction helped us calculate the retained austenite content. During the test, the scanning range was 40–100°, the scanning speed was 3°/min, the working voltage was 40 kV and the current was 40 mA.

$$f = \frac{1.4 I_y}{1.4 I_\gamma + I_\alpha} \tag{1}$$

In the formula, f is the content of retained austenite, I_γ is the integrated intensity of the characteristic peaks of

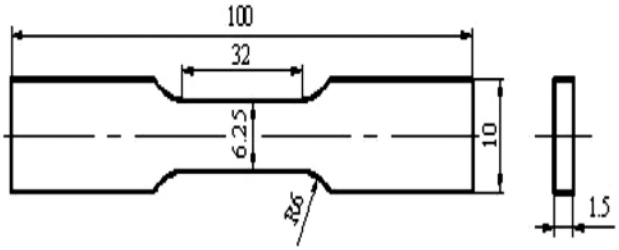

Figure 2: Tensile specimen dimensions for the experiment (mm)

austenite (200), (220), (311) and I_α is the integrated intensity of the characteristic peaks of ferrite (200), (211).

The experiment used a single-axis universal testing machine to test the mechanical properties and its model was WDW-100E.

The experiment used a single-axis universal testing machine to test the mechanical properties and its model was WDW-100E. The maximum load was 100 kN and the tensile rate was 2.0 mm/min. The tested steel was prepared according to the ASTM E8 standard for tensile specimens, as shown in **Figure 2**.

3 RESULTS AND DISCUSSION

3.1 Influence of the Q&P process and C-Mn partitioning on the microstructure

Figure 3 shows SEM images of the tested steel processed in different ways (the C partitioning time was 30 s). **Figure 3a** includes a SEM image of the Q&P tested steel, while **Figure 3b** includes a SEM image of the microstructure of the C-Mn partitioning steel. This microstructure obtained with the two processes consists of lath martensite, dispersed ferrite and some bainite. The formation of ferrite and bainite is due to the transfer of the tested steel to the salt-bath furnace where the temperature drops to the two-phase zone and the cooling rate is slow. When calculating the ferrite content with the image-processing software, we find that the content of the ferrite after the Q&P process is about 14.9 % and the content of the ferrite after the C-Mn partitioning process is about 18.8 %. Compared with the Q&P process, the content of ferrite increased by 3.9 % after the C-Mn partitioning. This is mainly due to the diffusion of the Mn atoms during C-Mn partitioning, leading to an uneven diffusion of Mn in the two-phase zone. The diffusion of atoms is not fully homogenized when they are subsequently austenitized at temperatures higher than 940 °C because a short dwell time cannot eliminate the uneven diffusion of Mn atoms. Hence, the austenite stability in some Mn-rich regions is significantly higher than that in Mn-scarce regions. During the subsequent transformation, due to the temperature dropping into the two-phase zone, the austenite with some Mn-scarce regions is easier to transform into ferrite, leading to an increase in the content of ferrite after the C-Mn partitioning process. **Figure 3** shows that some martensite orientations after the Q&P process are chaotic and diversified. However,

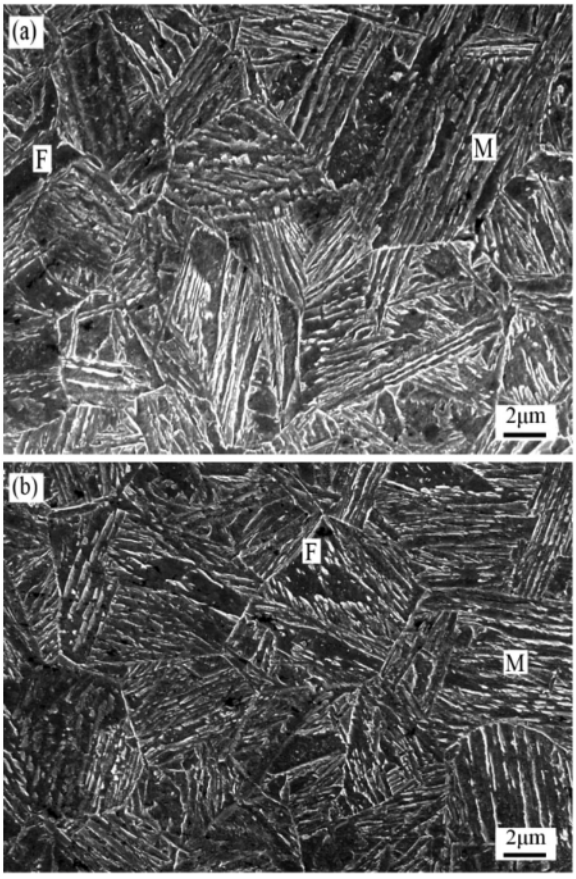

Figure 3: SEM images of two kinds of tested steel: a) Q&P steel, b) C-Mn partitioning steel

after the C-Mn partitioning treatment, some martensite orientations tend to be consistent, inducing microcracks at the grain boundaries of the tensile test. This is not conducive to the mechanical properties of the tested steel.

3.2 Influence of the C-Mn partitioning on the diffusion of C and Mn atoms

Figures 4 shows the EPMA mappings of the steel treated with C-Mn partitioning (the C-partitioning time was 30 s). **Figure 4** shows that both C and Mn atoms are enriched after the C-Mn partitioning process. The enrichment is more obvious in the yellow zones than green and blue zones. X. Y. Ding et al. performed EPMA characterization on the tested steel treated by Q&P process.[21] Compared with the Q&P process, the diffusion of C and Mn during the C-Mn partitioning was uneven. The atom enrichment is more evident after the C-Mn partitioning process, which shows that it affected the diffusion of Mn atoms. The Mn-rich areas in the tested steel obtained during the C-Mn partitioning process are consistent with the C-rich regions, and the Mn-scarce regions are also the C-scarce regions. This is mainly due to the Mn-atom diffusion providing a "channel" for the C atoms. Mn atoms are gradually enriched in the austenite regions in the two-phase zone. The Mn atom is a kind of replacement

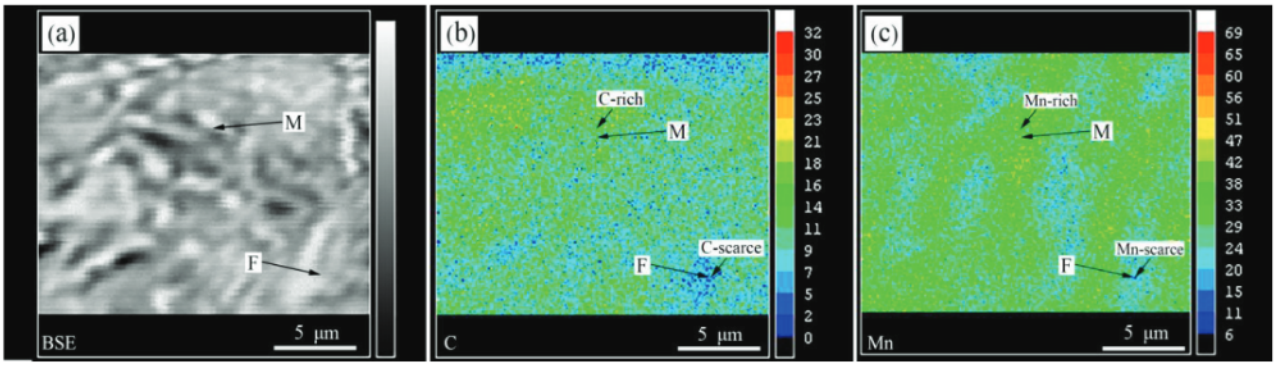

Figure 4: EPMA mappings of the tested steel treated with C-Mn partitioning: a) microstructure, b) C-atom distribution, c) Mn-atom distribution

atom,[22] larger than the Fe atom or C atom. Furthermore, the diffusion of C atoms and Mn atoms causes lattice distortions. As C atoms are interstitial atoms, they are easier to diffuse into the lattice gaps around a "channel" created by the diffusion of the Mn atoms, resulting in an enrichment of the C atoms around the Mn atoms. Although fully austenitized, the "channels" still exist. In the subsequent C-partitioning process, the C atoms are enriched in the "channels" created again by the Mn atoms, so that Mn-rich areas are also C-rich areas.

Besides, **Figure 4** shows that after the C-Mn partitioning process, the atom concentration of the tested steel in the center of the martensite is significantly higher than along the boundary. The schematic diagram in **Figure 5**[21] can intuitively describe the cause of this phenomenon. When the tested steel is heated above the A_{C1}, austenite gradually begins to nucleate. Mn atoms gradually accumulate in the boundary regions between ferrite and austenite. Mn atoms diffuse faster in ferrite and slower in austenite.[23] The Mn atoms in the edge area (**Figure 5b**) increase, causing the formation of a high Mn-atom content in the edge region and a low Mn-atom content in the center area of ferrite. The enrichment of Mn atoms at the boundaries also hinders the growth of the grain boundaries.[24,25] Although austenite grains are small, they are rich in manganese. With the progress of Mn partitioning, grain boundaries of austenite gradually migrate into ferrite and Mn atoms gradually diffuse into austenite grains. The subsequent complete austenitization of the tested steel does not fully homogenize the uneven diffusion of Mn atoms because of the short dwell time. In the subsequent quenching of the tested steel, martensite still retains an obvious C and Mn enrichment in the central region and a weak C and Mn enrichment at the boundaries.

3.3 XRD analysis of the Q&P process and C-Mn partitioning

Figure 6 shows the XRD patterns of the Q&P steel and C-Mn partitioning steel (the C-partitioning time was 30 s). The retained-austenite volume fraction of the tested steel obtained with the Q&P process was 0.71 %. The volume fraction of retained austenite of the tested steel obtained with C-Mn partitioning was 1.24 %.[26] The volume fraction of retained austenite in the C-Mn partitioning steel and Q&P steel was low. However, the volume fraction of retained austenite obtained with C-Mn partitioning increased significantly compared with the Q&P process. The main reason for this was the fact that the contents of C and Mn in the composition of the tested steel were not high, just 0.11 % and 1.50 %, respectively. The two elements were the key elements determining the stability of retained austenite at room tem-

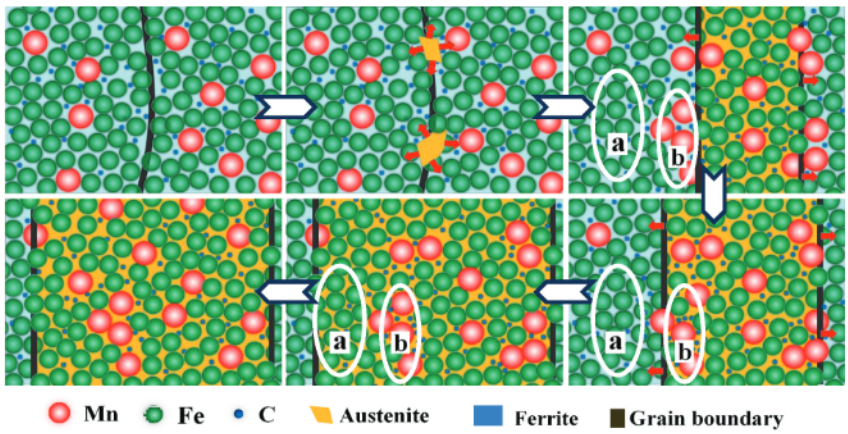

Figure 5[21]**:** Schematic diagram of manganese partition in the two-phase region

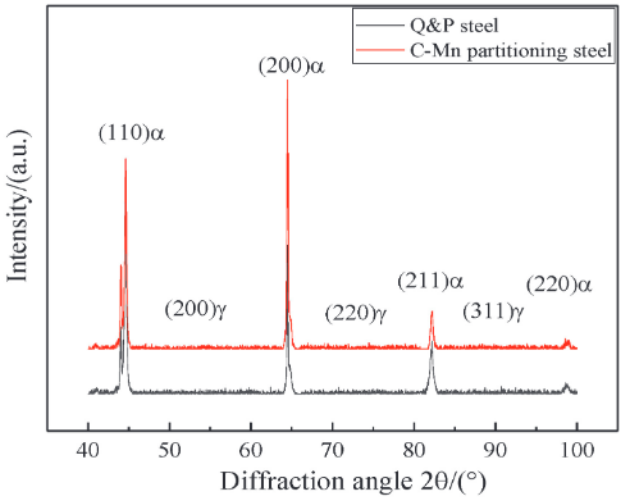

Figure 6: XRD patterns of the Q&P steel and C-Mn partitioning steel

perature. This resulted in the low volume fraction of retained austenite in the two tested steels at room temperature.

Moreover, because both methods produced some ferrite, the content of retained austenite at room temperature was low. Very little retained austenite can be observed in the SEM images. As mentioned above, the C-Mn partitioning process promotes the Mn-atom diffusion and Mn-rich areas are also C-rich areas. The stability of austenite in the atom-rich regions is better and easier to retain atroom temperature. As a result, the volume fraction of retained austenite must be increased by the C-Mn partitioning process.

3.4 Analysis of the mechanical properties and fracture morphology after the Q&P process and C-Mn partitioning

Figure 7 shows the mechanical properties of the Q&P steel and C-Mn partitioning steel. **Figure 7b** compares the PSEs of the two processes. The PSEs of the tested steel exposed to the two processes first increased and then decreased with the increase in the carbon-partitioning time. Generally speaking, the tensile strength of the tested steel obtained with C-Mn partitioning is low. But this steel exhibits a better performance than the steel obtained with the Q&P process in terms of the PSE and elongation. When the carbon-partitioning time is 20 s, the tensile strength of C-Mn partitioning can reach 995.7 MPa; the elongation after fracture can be 14.8 %; the PSE can reach 14.7 GPa·%.

The decrease in the tensile strength may be due to the increase in the ferrite content during C-Mn partitioning. Moreover, it is shown by the SEM image in **Figure 3** that the martensite orientation from the C-Mn partitioning steel may be different from the tensile direction, resulting in a partial decrease in the tensile strength. The tensile strength of the tested steel obtained with C-Mn partitioning is increased to a certain extent after 30 s. This may be due to the precipitation of some carbides with the increasing C-partitioning time.[27] The elongation after fracture of the two tested steels first increased and then decreased. Still, the fracture elongation of the Q&P treated steel is the best after 30-s C partitioning and the fracture elongation of the C-Mn partitioning steel is the best after 20 s C partitioning. This may be so because the enrichment of C by the C-Mn partitioning process is better due to the enrichment of Mn. XRD patterns of the two methods in **Figure 6** show that the volume fraction of retained austenite of the tested steel exposed to the two processes is relatively low. However, the C-Mn partitioning process makes the retained austenite more stable, and the steel treated in this way exhibits better mechanical properties.

Figure 8 shows the tensile fracture morphology of the Q&P steel and C-Mn partitioning steel. The dimple morphology of the steel tested with the Q&P process and C-Mn partitioning is elliptical, showing ductile fracture characteristics. It shows that a ductile fracture has a substantial effect on load absorption in crack propagation.[28] However, the difference is that the diameter of the dimple at the fracture obtained with the Q&P process is relatively small and different. On the other hand, the dimple of the steel tested with C-Mn partitioning is relatively

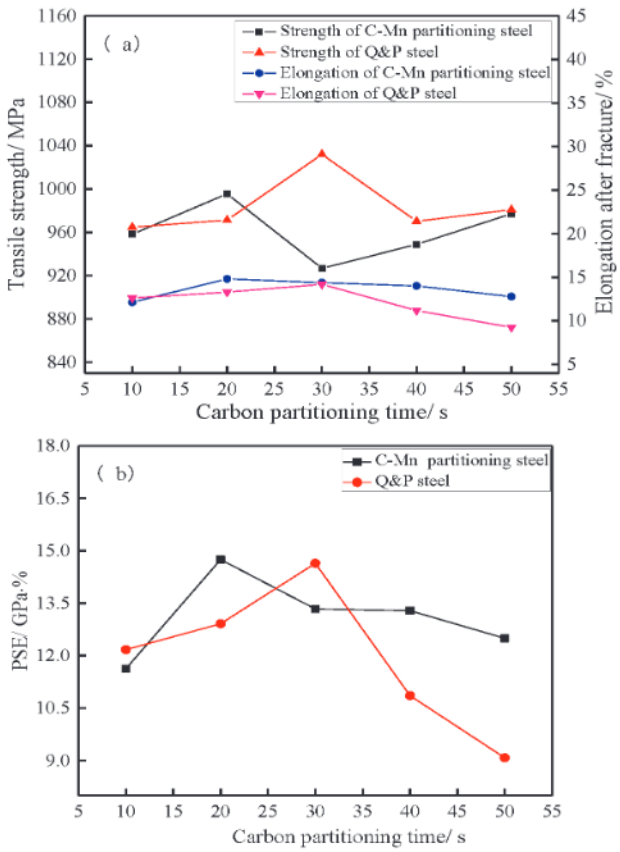

Figure 7: Comparison of the mechanical properties between the Q&P steel and C-Mn partitioning steel: comparison of the tensile strengths and elongations, b) comparison of the PSEs

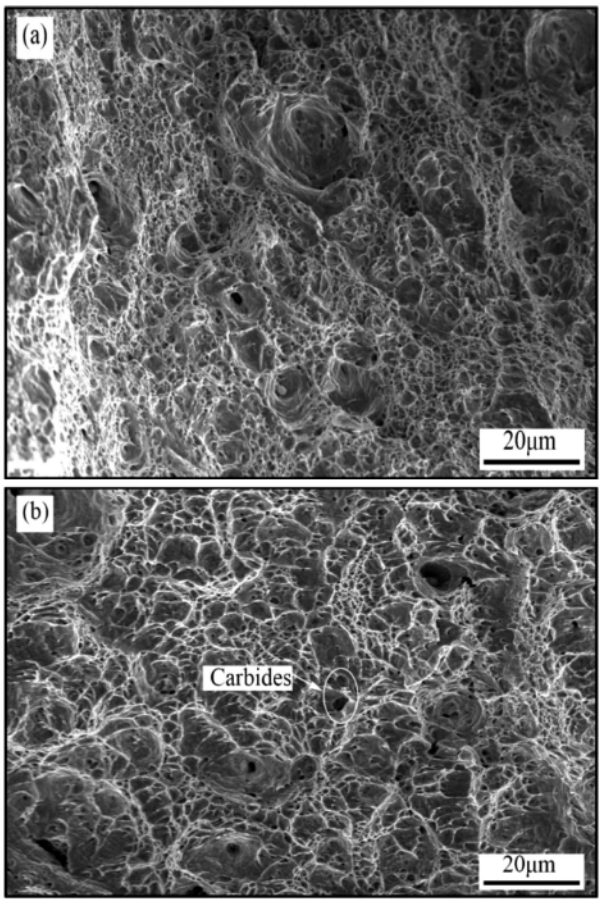

Figure 8: Tensile-fracture morphology of the tested steel: a) Q&P steel, b) C-Mn partitioning steel

large, its distribution is relatively uniform and second-phase particles can be observed.

The formation of dimples is mainly due to the nucleation, growth, aggregation, and fracture of tiny cavities. The diameter and depth of dimples have some influence on the mechanical properties of the material. Plasticity is directly proportional to the depth and diameter of the dimples. If a material has poor plasticity, second-phase particles are randomly distributed, and dimples have small diameters and lower depths.[29] Therefore, the plasticity of the C-Mn partitioning steel is more obvious than that of the Q&P steel. The carbides in **Figure 8b** (inside the ellipse) are Fe_3C.[30] Fe_3C appeared after 30 s of C partitioning, also reflecting the C-enrichment apparent effect caused by Mn partitioning. Due to the pinning effect of the second phase on the dislocations, the deformation was more difficult, increasing the tensile strength of the steel after 30 s of C partitioning.

4 CONCLUSIONS

1. The microstructures of the Q&P steel and C-Mn partitioning steel comprise a lot of lath martensite and scattered ferrite; the ferrite content of the C-Mn partitioning steel is slightly increased. The enrichment of C and Mn in the C-Mn partitioning steel is relatively obvious, Mn-rich areas are also C-rich areas. The volume fractions of retained austenite are relatively small after the two processes. Still, the volume fraction of the retained austenite in the C-Mn partitioning steel is significantly higher than that of the Q&P steel.

2. In terms of mechanical properties, the C-Mn partitioning steel has the best mechanical properties when the C-partitioning time is 20 s; then the tensile strength can reach 995.7 MPa, the elongation after fracture can reach 14.8 % and the product of strength and elongation can be 14.7 GPa·%. The C-Mn partitioning steel has advantages over the Q&P steel in terms of the elongation after fracture and PSE.

3. According to the fracture-morphology analysis, the dimples at the fractures of both the Q&P steel and C-Mn partitioning steel are round or elliptical, showing ductile-fracture characteristics. Compared with the Q&P steel, the C-Mn partitioning steel has relatively larger dimple depth and diameter, and here carbides appear as well.

Acknowledgment

This work was supported by the National Natural Science Foundation of China (No.51871136) and the Key Research and Development Project of the Shandong Province (2019GGX104057, 2019JMRH 0306).

5 REFERENCES

[1] Z. Wang, P. Liu, Y. Xu, Y. L. Wang, Y. S. Zhang, Hot Stamping of High Strength Steel with Tailored Properties by Two Methods, Procedia Engineering, 81 (**2014**) 1725–1730, doi:10.1016/j.proeng.2014.10.221

[2] N. Pornputsiri, K. Kanlayasiri, Effect of bending temperatures on the microst-ructure and springback of a TRIP steel sheet, Defence Technology, 16 (**2020**) 5, 980–987, doi:10.1016/j.dt.2019.11.018

[3] N. K. Tewary, S. K. Ghosh, D. Chakrabarti, S. Chatterjee, Deformation behaviour of a low carbon high Mn TWIP/TRIP steel, Materials Science and Technology, 35 (**2019**) 12, 1483–1496, doi:10.1080/02670836.2019.1630087

[4] X. H. Han, C. L. Wang, Y. Y. Li, G. Liu, Effects of quenching and partitioning process on mechanical properties of TRIP780 steel, Journal of Iron and Steel Research International, 26 (**2019**) 9, 991–999, doi:10.1007/s42243-018-0183-3

[5] J. Speer, D. K. Matlock, B. C. D. Cooman, J. G. Schroth, Carbon partitioning into austenite after mar- tensite transformation, Acta Materialia, 51 (**2003**) 9, 2611–2622, doi:10.1016/S1359-6454(03)00059-4

[6] B. Hu, H. Luo, F. Yang, H. Dong, Recent progress in medium-Mn steels made with new designing strategies, a review, Journal of Materials Science & Technology, 12 (**2017**) 1457–1464, doi:CNKI:SUN:CLKJ.0.2017-12-003

[7] Z. Y. Xu, A briefi introduction to quenching-partitioning-tempering (Q-P-T) process, Heat Treatment of Metal, 34 (**2009**) 6, 1–8, doi:10.13251/j.issn.0254-6051.2009.06.002

[8] T. Lin, H. W. Song, S. H. Zhang, M. Cheng, W. J. Liu, Y. Chen, Microstructure, Mechanical Properties, and Toughening Mechanisms of a New Hot Stamping-Bake Toughening Steel, Metallurgical and Materials Transactions A, 46 (**2015**) 9, 4038–4046, doi:10.1007/s11661-015-3020-3

[9] M. L. Li, H. Jiang, Y. L. He, L. B. Chen, G. T. Zhang, H. Wang, X. G. Lu, L. Li, Effect of two-step cooling process on mechanical properties of TRIP steel with high performance, Journal of Iron and Steel Research, 25 (**2018**) 4, 426–432, doi:10.1007/s42243-018-0039-x

[10] Y. F. Shen, X. X. Dong, X. T. Song, N. Jia, Carbon content-tuned martensite transformation in low-alloy TRIP steels, 9 (**2019**) 1, 1391–1409, doi:10.1038/s41598-019-44105-6

[11] J. Cramer, D. Adams, M. P. Miles, D. T. Fullwood, E. R. Homer, T. Brown, R. K. Mishra, A. Sachdev, Effect of strain path on forming limits and retained austenite transformation in Q&P 1180 steel, Materials Science & Engineering A, 734 (**2018**) 192–199, doi:10.1016/j.msea. 2018.07.062

[12] Q. He, Y. F. Wang, M. S. Wang, F. J. Guo, Y. Wen, C. X. Huang, Improving strength-ductility synergy in 301 stainless steel by combining gradient structure and TRIP effect, Materials Science & Engineering A, 780 (**2020**) 139–146, doi:10.1016/j.msea.2020.139146

[13] Y. J. Li, D. Liu, D. Chen, J. Kang, X. H. Wang, G. Yuan, R. D. K. Misra, G. D. Wang, Response of retained austenite to quenching temperature in a novel low density Fe-Mn-Al-C steel processed by hot rolling-air cooling followed by non-isothermal partitioning, Materials Science & Engineering A, 753 (**2019**) 197–207, doi:10.1016/j.msea.2019.03.043

[14] X. L. Gu, Y. B. Xu, F. Peng, R. D. K. Misra, Y. Wang, Role of martensite/austenite constituents in novel ultra-high strength TRIP-assisted steels subjected to non-isothermal annealing, Materials Science & Engineering A, 754 (**2019**) 318–329, doi:10.1016/j.msea.2019.03.070

[15] M. Gouné, S. Aoued, F. Danoix, G. Geandier, A. Poulon-Quintin, J. C. Hell, M. Soler, S. Y. P. Allain, Alloying-element interactions with austenite/martensite interface during quenching and partitioning of a model Fe-C-Mn-Si alloy, Scripta Materialia, 162 (**2019**) 181–184, doi:10.1016/j.scriptamat.2018.11.012

[16] C. H. Song, H. Yu, L. L. Li, J. Lu, Effect of carbon at interface of austenite on manganese segregation of low carbon and manganese steel, Materials Letters, 174 (**2016**) jul.1, 75–78, doi:10.1016/j.matlet.2016.03.090

[17] Y. Q. Tian, G. Tian, X. P. Zheng, Y. L. Wei, J. Y. Song, L. S. Chen, Influence of C and Mn elements on stability of retained austenite in quenching and partitioning bainitic steel, Heat Treatment of Metals, 44 (**2019**) 07, 112–116, doi:10.13251/j.issn.0254-6051.2019.07.024

[18] S. Qin, Y. Liu, J. Z. Zhang, Y. Wang, Y. H. Rong, X. W. Zuo, N. L. Chen, Approach and mechanism of toughness enhancement for a high carbon Q-P-T steel, 1 (**2019**) 1–2, 11–16, doi:10.1080/25787616.2018.1560160

[19] N. Maheswari, S. G. Chowdhury, K. C. H. Kumar, S. Sankaran, Influence of alloying elements on the microstructure evolution and mechanical properties in quenched and partitioned steels, Material science & Engineering A, 600 (**2014**) 10, 12–20, doi:10.1016/j.msea. 2014.01.066

[20] E. Emadoddin, A. Akbarzadeh, R. Petrov, L. Zhao, Anisotropy of Retained Austenite Stability during Transformation to Martensite in a TRIP-Assisted Steel, Steel Research International, 84 (**2013**) 3, 297–303, doi:10.1002/srin.201200197

[21] C. N. Jing, X. Y. Ding, D. M. Ye, J. R. Zhao, T. Lin, S. B. Xu, Effect of Different Isothermal Time on Microstructure and Mechanical Property of the Low-Carbon Steel Treated by Dual-Stable C-Mn partitioning Process, Scanning, 2020 (**2020**) 1–11, doi:10.1155/2020/5931721

[22] H. T. Jiang, B. T. Zhuang, X. G. Duan, Y. X. Wu, Z. X. Cai, Element distribution and diffusion behavior in Q&P steel during partitioning, International Journal of Minerals, Metallurgy, and Materials, 20 (**2013**) 11, 1050–1059, doi:10.1007/s12613-013-0833-1

[23] Y. Q. Tian, H. J. Zhang, L. S. Chen, J. Y. Song, Y. Xu, S. H. Zhang, Effect of alloy elements partitioning behavior on retained austenite and mechanical property in low carbon hihg strength steel, Acta Metallurgica Sinica, 50 (**2014**) 5, 531–539, doi:10.3724/SP.J.1037.2013.00709

[24] Y. Q. Tian, R. Li, J. Y. Song, Y. L. Wei, X. Dai, L. S. Chen, Effect of Mn Partitioning Time on Microstructure and Properties of Low-carbon Steel with I&Q&P Treatment, Hot Working Technology, 45 (**2016**) 16, 161–164, doi:10.14158/ j.cnki.1001-3814.2016.16.041

[25] A. Bhattacharya, P. K. Bokinala, R. Mitra, D. Chakrabarti, Relative effect of C and Mn on strength-toughness of medium Mn steels, Materials Science & Technology, 35 (**2018**) 1, 1–13, doi:10.1080/02670836.2018.1537609

[26] M. T. Liang, Y. F. Shen, W. Y. Xue, X. C. Lu, Influence of quenching and partitioning on microstructure and mechanical properties of a Cu-TRIP steel, Materials Science and Technology, 25 (**2017**) 1, 50–55, doi:10.11951/j.issn.1005-0299.20160206

[27] H. Chen, L. J. Wei, Z. J. Xie, X. M. Wang, C. J. Shang, Carbide precipitation and hydrogen embrittlement susceptibility of a 960 MPa grade ultra-high strength steel, Materials Technology, 34 (**2018**) 2, 1–10, doi;10.1080/ 10667857.2018.1536343

[28] I. M. Sas-Boca, D. Frunză, F. Popa, D. A. Ilutiu-Varvara, M. C. Tintelecan, Influence of Temperature and Strain Rate on Microstructure and Fracture Mechanism of Mild Steel, Procedia Manufacturing, 46 (**2020**) 891–898, doi:10.1016/j.promfg.2020.05.005

[29] I. Konovalenko, P. Maruschak, O. Prentkovskis, Automated Method for Fractographic Analysis of Shape and Size of Dimples on Fracture Surface of High-Strength Titanium Alloys, Metals, 8 (**2018**) 3, 161, doi:10.3390/met8030161

[30] Z. B. Dai, Z. G. Yang, C. Zhang, H. Chen, Incomplete carbon partitioning during quenching and partitioning of Fe-C-Mn-Si steels: Modeling and experimental validations, Acta Materialia, 200 (**2020**) 597–607, doi:10.1016/j.actamat.2020.09.045